Understanding spontaneous orientation polarization of amorphous organic semiconducting films and its application to devices

Yutaka Noguchi [a],[*], Yuya Tanaka [b],[c],[1], Hisao Ishii [b],[c], Wolfgang Brütting [d]

[a] *School of Science & Technology, Meiji University, Kawasaki, Japan*
[b] *Center for Frontier Science, Chiba University, Chiba, Japan*
[c] *Graduate School of Science and Engineering, Chiba University, Chiba, Japan*
[d] *Institute of Physics, University of Augsburg, Augsburg, Germany*

ARTICLE INFO

ABSTRACT

Spontaneous orientation polarization (SOP) of amorphous organic semiconducting films has attracted much attention because of its frequent observation in common organic light-emitting diodes (OLEDs) and potential influences on the device properties of OLEDs. On the other hand, the formation mechanism of SOP has been controversial for a long time, ever since its discovery in 2002. Recently, the formation mechanism of SOP was explained in terms of the surface equilibration mechanism of vapor-deposited glasses, and the understanding of SOP has progressed significantly. Based on the improved understanding, some active control methods of SOP have been demonstrated and further influences on the device performance of OLEDs were revealed, suggesting that higher efficiency can be achieved by managing SOP properly. Furthermore, some applications of SOP have also been proposed, such as a self-assembled electret and a tool for evaluating materials properties. In this paper, recent progress in the understanding of SOP and its applications to devices are reviewed.

1. Introduction

1.1. Brief history of SOP

Spontaneous orientation polarization (SOP) of organic semi-conducting films was discovered as giant surface potential (GSP) of an Alq$_3$ film evaporated on a gold substrate [1]. GSP grows linearly as a function of the film thickness without saturation, e.g., reaching as high as 28 V at 560 nm for Alq$_3$, and surprisingly it exceeds far beyond the Mott-Schottky limit of metal-semiconductor interfaces at thermal equilibrium. SOP originates from the alignment of the permanent dipole moment (PDM) of the molecules, and the linear growth of GSP corresponds to a constant orientation degree of the PDMs on average, given as $\langle \cos\theta_p \rangle$, where θ_p is the tilt angle with respect to the surface normal. The constant polarization results in a fixed density of polarization charge at the hetero interfaces in stacked multilayer devices, such as organic light-emitting diodes (OLEDs) [2–4]. Interestingly, such interface charge had already been found in a typical bilayer OLED consisting of Alq$_3$ and NPB in 2000 [5–7], that is two years earlier than the first report of GSP. These two phenomena were concluded to have the same origin, namely SOP, in 2008 [2]. Since then, SOP has been found frequently in evaporated films of common OLED materials [3,4,8–10], and it was pointed out to have influences on the device performance of OLEDs, such as charge injection, accumulation, and degradation [3,11–20]. Currently, SOP is considered as an important factor to optimize the device performance of OLEDs [4,21].

Although 20 years have passed since the discovery of SOP in organic semiconducting films, the formation mechanism of SOP has been controversial for many years. The main reasons can be attributed to the photoinduced decay nature of GSP and the overall small orientation degree of PDMs. Since it has been known that GSP decays via light absorption of the film [1,22–25], one has to carefully examine the properties of SOP and, in doing so, avoid light illumination in case of measuring the surface potential. In addition, although a huge potential is built up across the film, the averaged orientation degree of the molecule's PDM is typically small, that is, $\langle\cos\theta_p\rangle \sim 0.05$ for Alq$_3$ [23]. This tiny averaged orientation degree makes accurate evaluation difficult. These circumstances have limited the experimental techniques being available for investigating SOP and prevented the understanding of the formation mechanism of SOP. Moreover, only a few molecules were known as exhibiting SOP other than Alq$_3$.

However, the fact that SOP is equivalent to an interface charge opened an opportunity to investigate SOP in devices [2–4], where the photoinduced decay can be ignored and SOP can be evaluated using conventional methods such as capacitance-voltage ($C–V$) measurement, displacement current measurement (DCM), and so on [4,26–28]. Furthermore, as many OLED materials exhibit SOP [4,10,21,29], it has been recognized as commonly inherent in actual OLEDs.

The fundamentals of SOP and its influences on the OLED properties investigated in earlier work have been published elsewhere [4].

1.2. Recent progress in understanding of SOP and its applications

In recent years, the understanding of the formation mechanism of SOP has significantly progressed; specifically SOP is formed as a result of partial equilibration at the asymmetric situation on the film surface during physical vapor deposition [30–32]. From a microscopic viewpoint, the mechanism can be understood as a balance of positive and negative factors for increasing polarization order [33,34], where the positive driving force is a short-range van der Waals (vdW) interaction between the outer part of the molecule and the film surface [33], while the negative counterpart is the PDMs' dipole-dipole interactions between molecules on the film surface [10,34,35]. The number of stable postures that the molecule can take on the film surface is also vital in terms of configurational entropy [36–39]. The current understanding of the formation mechanism of SOP is described in Section 2.1.

Based on the understanding of the formation mechanism, some methods to control SOP have been demonstrated. The molecular shape and the intermolecular interactions can be modified by attaching substituents to the outer part of the molecule, leading to significant changes in the molecular orientation of the resultant film [8,34,36,40–45]. On the other hand, SOP can be controlled by the evaporation conditions during the film deposition, such as substrate temperature [30,46,47],

deposition rate [30,48], and light illumination [49]. Guest-host systems are also very promising for tuning SOP [29,34,35,40,50,51]. Some active control methods are introduced in Section 2.2.

Because of its frequent observation in common OLED materials, the influences of SOP on device performance have been actively studied (Fig. 1) [46,47,52–54]. Using the active control method, the roles of SOP in the device performance of OLEDs have been examined. Bangsund et al. recently revealed that the hole accumulation due to SOP induces a significant triplet-polaron quenching (TPQ) at the interfaces affecting the emission layer (EML) below the turn-on voltage of device operation [46]. They demonstrated higher external quantum efficiencies (EQEs) of Ir(ppy)$_3$-based phosphorescent OLEDs by removing SOP. Similar enhancement of EQE was also found in an Alq$_3$-based fluorescent OLEDs [47]. In Section 3.1, the influence of SOP on EQE is discussed.

The interface properties of a device are modified by SOP, e.g., the charge accumulation at organic/organic interfaces can lead to emission zone confinement and modifies the carrier injection efficiency at the electrode/organic film interface [13,14,20,51,55]. Meanwhile, the electric field in a film formed by SOP induces spontaneous exciton dissociation [52,56,57]. Although the roles of SOP in the device performance and its optimization are still actively investigated; some studies on the SOP-related device properties are overviewed in Sections 3.2 and 3.3.

SOP has been used as a tool for evaluating material properties [29,40,50,58–61]. Züfle et al. proposed a metal-insulator-semiconductor-charge carrier extraction by linearly increasing voltage (MIS-CELIV [62]) measurement to determine the material's charge carrier mobility using a conventional OLED stack, where the SOP layer acts as an excellent charge blocking layer instead of conventional insulator materials [58]. In another case, Morgenstern et al. have proposed a method for accurate determination of molecular orientation based on the combined evaluation of PDM and transition dipole moment (TDM) orientations [50]. The combined analysis gives deep insights into the molecular orientation distribution and its formation mechanism [29,40,50,61]. These techniques are introduced in Section 4.1.

As a novel application of SOP, Y. Tanaka et al. recently proposed a vibrational energy generator (VEG) where TPBi is used as a "self-assembled electret (SAE)" [48,63,64]. SOP induces a significant density of polarization charge on the film surface, typically 1–2 mC/m^2. This value is as high as the polymer-based electrets after corona charging [65], which are widely used for microphones, sensors, and filters [66]. A distinctive advantage of the SAE is that it does not require any charging process during electret preparation. By utilizing this advantage, micro-electromechanical systems (MEMS) including post-processed SAE for VEG was demonstrated [67]. In Section 4.2, the recent studies of the VEGs using SAE are reviewed.

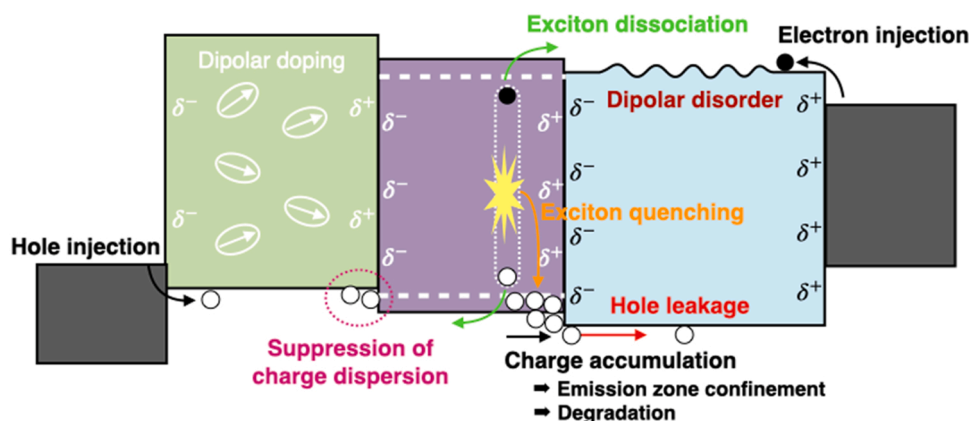Numerous studies on SOP have been reported during the last few

Fig. 1. Schematic illustration of possible influences of SOP on the properties of OLEDs. The suppression of charge dispersion and dipolar disorder relate to microscopic potential fluctuations induced by the random orientation distribution of PDMs rather than their macroscopic orientation ordering.

years by various research groups. Although 20 years have passed since the first GSP was reported, this research field has attracted considerable attention that is even growing recently. In this review, we summarize the current status of SOP and give future prospects of this research field.

2. SOP formation in amorphous organic semiconducting films

2.1. Dominant factors of SOP formation

Amorphous films of organic semiconducting materials have been used for stacked multilayer OLEDs [68], because of their smoothness and macroscopic homogeneity. Meanwhile, however, evaporated films of OLED materials often exhibit electrical and optical anisotropies due to molecular orientation [4,21,69,70]. The evaporated amorphous films of OLED materials are thus referred to as hybrid materials that combine some of the useful features of crystals and glasses [31].

Ediger et al. reported the surface equilibration mechanism that explains how anisotropy is an inherent feature of organic vapor-deposited glasses (Fig. 2) [30–32]. They pointed out that key is a high mobility of molecules at the surface of the growing film. When the molecules arrive at the film surface during the vacuum deposition, they move around on the surface even below the glass transition temperature (T_g) because of less interactions at the film surface than in the bulk. An anisotropic surface layer would thus be formed due to asymmetric molecular shape and molecular interactions at the surface region facing to the vacuum side of the film (Fig. 2) [30,41]. Subsequent deposition covers the mobile surface molecules and causes the anisotropic surface layer to be inherited in the bulk. Finally, anisotropic amorphous films are formed. This surface equilibration mechanism has been applied to explain the formation of SOP in Alq$_3$ [30]. As the mechanism suggested, anisotropy is a specific feature of vapor-deposited glasses, and it disappears in solution processed films of the corresponding materials [32,71,72].

Based on an atomic Monte Carlo model that mimics the molecular deposition process, Friederich et al. demonstrated that the simulated GSP values of several materials are consistent with those determined experimentally [33]. They pointed out that short-range vdW interactions dominate the anisotropic orientation of the molecule at the growing film surface, rather than the electrostatic PDM interaction between molecules. Accordingly, the shape and the outermost parts of the molecule, that determine the vdW interaction with the film surface, play a crucial role to form SOP. The anisotropy of the surface layer is
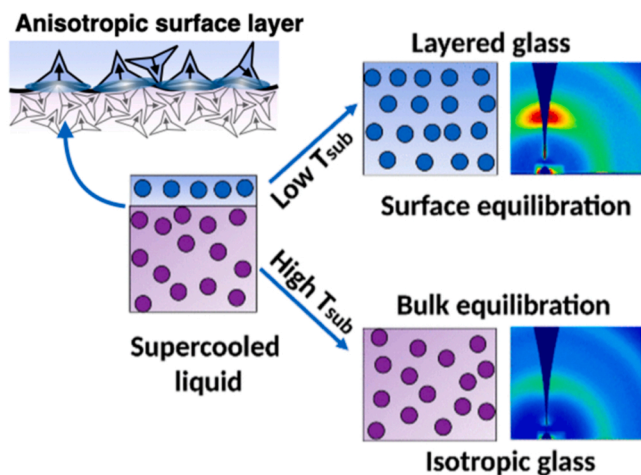
attributed to an ensemble of molecular configurations, where their statistic distribution is determined by their stability and possible variations. This scenario can be considered as a modified "asymmetric dice model" proposed by Isoshima et al. [36].

The electrostatic dipole-dipole interaction between PDMs also plays an important role, though it works as a negative factor for the SOP formation [10,34,35,50]. Several experimental results have been reported that the averaged orientation degree of PDM is enhanced in mixed films with nonpolar host materials. Accordingly, resultant SOP can even be greater in mixtures by diluting PDM densities, since the dipole-dipole interaction decays with increasing the intermolecular distance, whereby the nonpolar host acts as a spacer (Fig. 3). In other words, SOP is significantly quenched in a neat film by taking antiparallel configurations of PDMs for reducing the electrostatic interaction energy [35].

The SOP formation would eventually result from a balance of positive and negative driving forces (Fig. 4), where the positive factor is the vdW interaction between the outermost part of the deposited molecule and the film surface, and the negative factor is the PDM interaction between molecules on the film surface. Noguchi et al. have reported the GSP characteristics of TPBi films deposited on a Au substrate with and without surface treatment by a self-assembled monolayer (SAM) of dodecanethiol (Fig. 4(a)) [34]. The surface potential of the film deposited on the SAM-treated Au substrate is smaller than that deposited on the untreated substrate. On the untreated Au, the deposited molecules do not travel over a long distance because of the strong interaction with the substrate surface (Fig. 4(f)). Consequently, the molecules immediately cover the substrate surface (Fig. 4(b) and 4(c)), and the surface potential grows linearly from the thin-film region. On the other hand, the SAM-treated Au has a smaller surface free energy, that is, the vdW interaction on the substrate surface is suppressed. The deposited molecules likely form clusters because of long-distance travel on the surface (Fig. 4(d), (e), and (g)). The PDM interaction becomes relatively dominant, and consequently, the SOP formation was suppressed. However, after the molecules have completely covered the SAM-treated surface, the surface potential grows as well as in the untreated sample.

Fig. 2. Illustration of the surface equilibration model. An anisotropic surface layer is formed due to the asymmetric molecular shape and interactions at the vacuum/film interface. The anisotropic structure is inherited into the bulk at low substrate temperatures, though the layer structure disappears at higher substrate temperatures. Adapted with permission from Ref. [30]. Copyright 2019, American Chemical Society.

Fig. 3. Orientation degree of Alq$_3$'s PDM in a mixed film of Alq$_3$ and NPB, where the PDM of Alq$_3$ (p) is assumed to be 3.9 D. The inset figures show the molecular structures of Alq$_3$ and NPB, and their schematics. The sketches on the top show the situation for two interacting PDMs on the surface of the mixed (left) and neat (right) films. U_p is the electrostatic potential, and r_{Alq} is the distance between two PDMs. Adapted from Ref. [35] under the terms of the CC-BY 4.0 license. Copyright 2016, Authors.

Fig. 4. (a) Surface potentials of TPBi neat films deposited on Au with/without surface treatment with a dodecanethiol (C12T) self-assembled monolayer (SAM). The chemical structure of TPBi is also shown. (b)–(e) Atomic force microscopy images of TPBi films. Each image corresponds to the surface of a film indicated in panel (a). The scale bar is 2 μm. The height range is 6 nm for panels (b), (c), and (e) and 20 nm for panel (d). (f) and (g) Schematic illustrati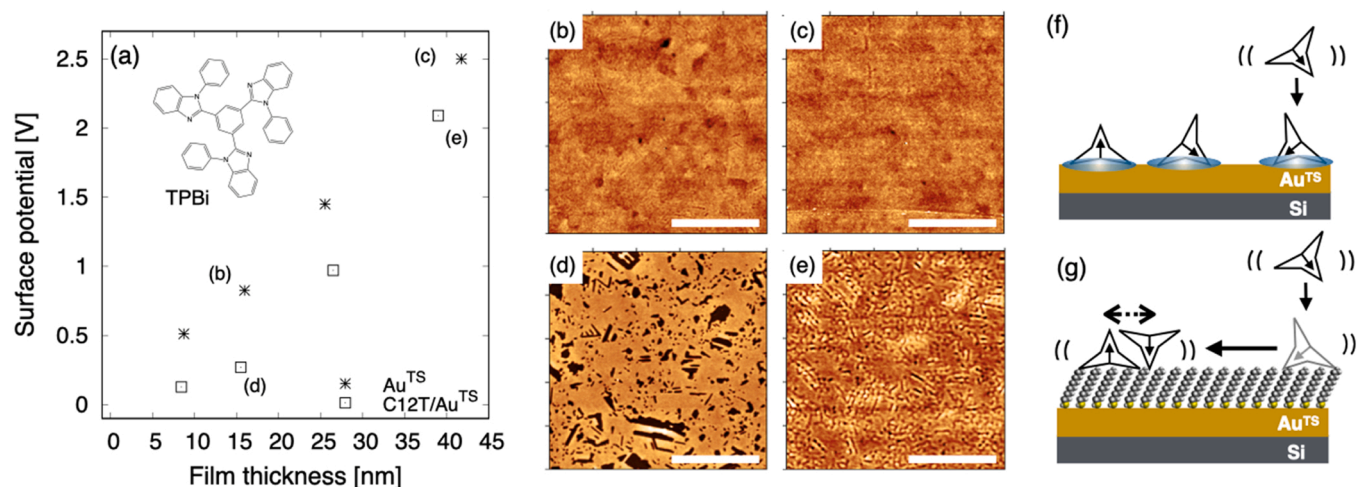ons of the influence of the substrate surface. A smooth film is formed on the bare Au substrate, because of the strong interaction between the molecule and the substrate (f). On the other hand, clusters are formed on the SAM-treated substrate, because the PDM interaction between the molecules becomes relatively dominant (g). Adapted with permission from Ref. [34]. Copyright 2021, John Wiley & Sons, Inc.

2.2. Active control methods of SOP

As suggested in the surface equilibration mechanism, SOP depends on the evaporation conditions, such as the substrate temperature and the deposition rate [30–32]. SOP decreases with increasing substrate temperature during film deposition (Fig. 5) [30,46,47], and it finally disappears at temperatures above T_g. Meanwhile, it has been reported that a faster deposition rate of TPBi results in larger SOP in the resultant film [48]. The GSP of the TPBi film deposited at 4.0 Å/s (65.4 mV/nm) becomes 1.8 times higher than that at 0.2 Å/s. Bagchi et al. pointed out that a faster deposition rate by a factor of 7 has the same impact on the film structure as decreasing the substrate temperature by 10 K in the case of Alq_3 [30]. The molecules on the surface travel shorter at faster deposition rates before they are trapped by further deposition, and the occurrence of compensation of PDM may be suppressed. This situation is analogous to the lower substrate temperatures, where the mobility of the molecule on the surface becomes lower. Accordingly, a faster deposition rate results in the enhancement of SOP, as well as the deposition at a lower substrate temperature.
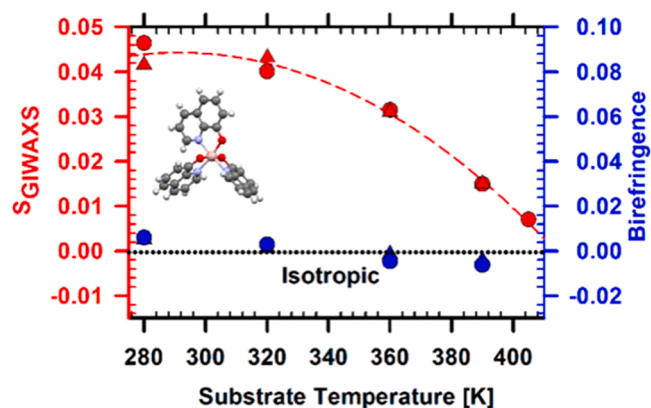
Recent studies have also revealed quantitative difference between the values of GSP slopes reported by several groups. For instance, the GSP slope of TPBi neat films has been reported ranging from 43 to 88 mV/nm [3,4,10,45,46,48,63]. This variation may originate from details of experimental conditions, such as the deposition rate, substrate temperature, substrate material, and so on. In addition, accurate evaluation of the film thickness is obviously important. As a standard procedure, the GSP slope has been evaluated by Kelvin probe as the thickness dependence of the surface potential of a vacuum-deposited film on an ITO or Au substrate at a deposition rate of ~1 Å/s. In many cases, the substrate temperature was not controlled, so that it may depend on the environment and configurations in the evaporation chamber. For quantitative discussions on relations to device properties, such details should be similar to the device fabrication conditions.

Y. Tanaka et al. reported that SOP of a TPBi film can be enhanced by non-polarized light illumination at a wavelength of 300 nm during film deposition [49]. In a bilayer device consisting of TPBi and NPB, they found that the interface charge density of the illuminated device is increased by 1.7 times of that in the control device fabricated in dark. The increase of the interface charge density can be attributed to the enhancement of molecular orientation, since the PDM interaction between the molecules would be attenuated by charge redistribution induced by the light illumination. An effect of light illumination on the interface charge density was also observed in an Alq_3-based bilayer device, though either enhancement of molecular orientation or trapped electrons could be responsible in this case [15].

In terms of molecular design, the molecular shape and the outermost part of the molecule would be important for the active control of SOP. For instance, $Al(7\text{-}prq)_3$ and $Al(q\text{-}Cl)_3$, which are derivatives of Alq_3 with modified ligands, show very large GSP slope of –103 and 94 mV/nm, respectively (Fig. 6(a)) [8,13,34,36]. These values are approximately double the GSP slope of Alq_3 (48 mV/nm), although the PDM magnitudes of these derivatives are even smaller than that of Alq_3. On the other hand, the GSP slope of $6FAlq_3$ is only 29 mV/nm [4], possibly due to the weak interaction of the fluorinated ligands and the film surface. Furthermore, Schmid et al. have reported molecular orientations (TDM orientations) of $Ir(dbfmi)_3$ and its multiple derivatives, where different functional groups were attached to the ligands (Fig. 6(b)–(e)) [40]. They demonstrated that the anisotropy of films varies depending on the aspect ratio and local electrostatic interactions of the dye molecule with the film surface during deposition. Jung et al. obtained similar

Fig. 5. Grazing incidence wide-angle X-ray scattering (GIWAXS) order parameter (red) and birefringence (blue) of Alq_3 films deposited at different substrate temperatures. The GIWAXS order parameter characterizes the structural anisotropy associated with molecular layering. Results for 260 nm (circles) and 540 nm (triangles) films are shown. Reproduced with permission from Ref. [30]. Copyright 2019, American Chemical Society.

Fig. 6. (a) Chemical structure of Alq$_3$, Al(7-prq)$_3$, Al(q-Cl)$_3$, and 6FAlq$_3$. The PDM magnitude and GSP slope of each molecule are also shown. (b) Chemical structures of Ir(dbfmi)$_3$ and its derivatives. For the compounds A-1–A-5, the imidazole group was modified with different alkyl chains. The dibenzofuran was modified for the materials B-1–B-3. (c) and (d) TDM orientation in dependence of the (c) molecular aspect ratios and the (d) difference between the maxima and mean values of the electrostatic surface potential of the dyes. (e) Schematic representation of the interaction of *fac*-Ir(dbfmi)$_3$ (left) and *fac*-A-5 (right) during the deposition process. In the case of *fac*-Ir(dbfmi)$_3$, the imidazole group is able to strongly interact with the previously deposited molecules, leading to a preferential alignment of the dye in the film. For *fac*-A-5, the imidazole group is shielded from its surrounding by the additional phenyl rings. This leads to an isotropic distribution of the molecules within the film. (b)–(e) Adapted with permission from Ref. [40]. Copyright 2020, ACS Publishing.

results of the roles of the ligands on molecular orientation, and demonstrated highly efficient Ir complex-based OLEDs owing to the enhancement of horizontal TDM orientation [43].

As another method, Wang et al. have recently reported the SOP enhancement by tuning molecular conformations [45]. They attached ethyl groups to the N-phenyl moieties of TPBi and eliminated a conformer with C_1 symmetry which contributes less to SOP than another conformer with C_3 symmetry. Here, the population of the conformer with C_3 symmetry is estimated to be 17% in the normal TPBi film, while it increases to 100% in their modified TPBi (*p*-ethyl-TPBi) film. As a result, the GSP slope of the *p*-ethyl-TPBi film was enhanced 1.8 times as compared to the normal TPBi film.

Recently, M. Tanaka et al. have demonstrated a molecular design concept to control SOP including its magnitude and polarity [44]. They employed trifluorometyl (CF_3) groups to define the molecular orientation, and attached it to the molecular backbone with other functional groups responsible for the magnitude and polarity of the PDM. Because of its weak vdW interaction, CF_3 groups are likely to appear at the vacuum side on the film surface. Based on this molecular design concept, they successfully controlled the GSP slope of the resultant films over a remarkably very wide range, both in the positive and negative directions.

It should be noted that although SOP has been frequently observed in the films of common OLED materials, their polarity is mostly positive, corresponding to positive polarization charge induced on the film surface. Specific reasons for such biased occurrence of positive SOP have not yet been understood in detail. Nevertheless, according to the formation mechanism of SOP and the molecular design proposed by M. Tanaka et al. [44], key would be the relative position of the functional groups responsible for the electronegativity (related to PDM) and the strong electrostatic interaction with respect to the molecular framework. These functional groups of common materials are often identical or located on the same side of the molecule since the majority of the functional groups consists of H, C, O, and N.

Another method to control SOP is to suppress the negative factor, that is, the PDM interaction, by diluting PDMs in the film with a nonpolar host [34,35,50,51]. As mentioned in Section 2.1, SOP is even enhanced in mixed films. Jäger et al. have proposed a concept of "dipolar doping", where SOP of the resultant film can be controlled as a function of the doping ratio of polar molecules [35]. They examined the interface charge density of bilayer devices, where the NPB films doped with Alq_3 were employed as an electron transport layer (ETL) (Fig. 7(a)). The

interface charge density (corresponding to the polarization charge density of SOP) induced by the doped layer varies significantly. The highest interface charge density is observed at a doping ratio of 50% and the value is about 17% higher than that of a neat Alq_3 film (Fig. 7(b)). Similar enhancement of SOP was observed for mixed films of TPBi and nonpolar host materials [34]. Fig. 7(c) shows the GSP slope of mixed films as a function of the TPBi ratio. Peaks appear at a TPBi content of 50% for the TCTA and CBP hosts similar to the Alq_3:NPB mixture, however not for the NPB host. The calculated intermolecular interaction energies suggest that NPB does not act as a good spacer for TPBi, unlike for Alq_3 and the other combinations of host and guest molecules [34,37].

3. Influences of SOP on OLED performance

3.1. Exciton quenching due to SOP

SOP induces excess charge accumulation at organic hetero interfaces, and their amount is comparable to the maximum total charge accumulated in a typical OLED under operation [4]. When the accumulation site is located at the EML interfaces, the accumulated charge would confine the emission zone [4,20,46,53], act as a quencher of excitons [46,47,54,73], and lead to a faster device degradation (Fig. 1) [4]. Importantly, such excess charge accumulation occurs at biases below the device turn-on voltage, indicating that their influences are included in the characteristics of the device, though it has not typically been taken into account.

Bangsund et al., have revealed TPQ by the accumulated holes due to SOP in Ir(ppy)$_3$-based OLEDs (Fig. 8), where TPBi is used as an ETL and as host of the EML [46]. Using lock-in detection of photoluminescence (PL), they evaluated the luminescence loss below turn-on to be more than 20%. Moreover, they demonstrated that the maximum EQE increases by more than 15% by eliminating SOP with substrate heating during deposition or using a negligible SOP material (B3PyMPM) instead of TPBi.

Similar enhancement of EQE by eliminating SOP has been observed in Alq_3-based bilayer OLEDs [47]. Esaki et al. have reported that the SOP of Alq_3 decreased by one half with increasing substrate temperature during deposition of Alq_3 from 260 to 328 K. The EQE of the resultant device increased by 40%. They assigned the contributions of the enhanced EQE as follows; improving PL quantum yield (PLQY) (3.7%), increasing outcoupling efficiency (10.5%), and eliminating singlet-polaron annihilation (~25%).
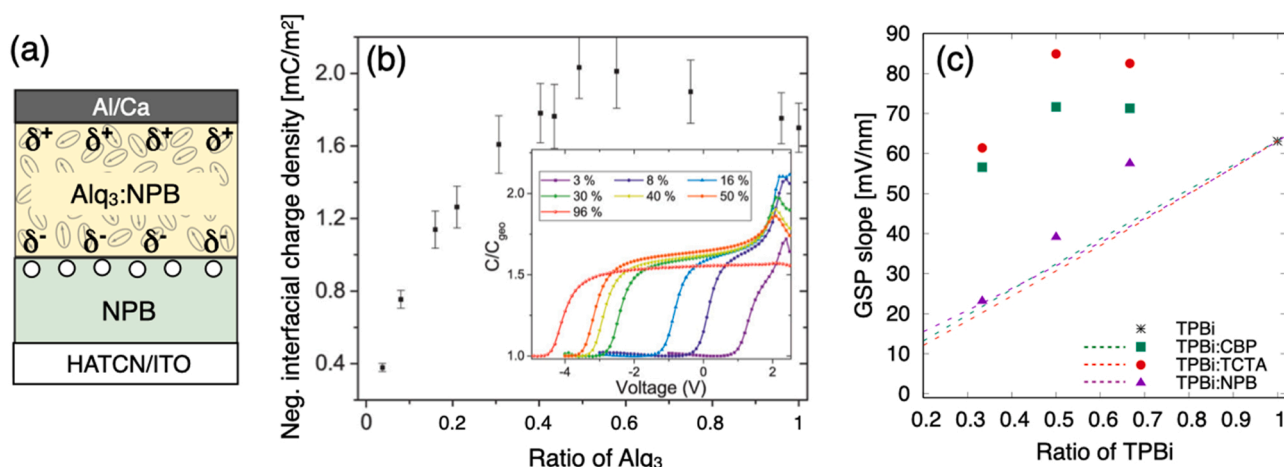
Fig. 7. (a) Schematic illustration of the device structure used for a "dipolar doping" bilayer device. (b) Interfacial charge densities for different Alq_3 doping ratios. The interface charge density was estimated from the capacitance-voltage curve of the bilayer device (inset). Reproduced from Ref. [35] under the terms of the CC-BY 4.0 license. Copyright 2016, Authors. (c) GSP slope of mixed films of TPBi and nonpolar host materials (CBP, TCTA, and NPB). Note that NPB is only slightly polar (0.34 D). The broken lines indicate the calculated GSP slopes by assuming the same orientation degree of TPBi as in a neat film. Reproduced from Ref. [34]. Copyright 2021, John Wiley & Sons, Inc.

Fig. 8. (a) Device structure of the Ir(ppy)$_3$-based OLED. The EML and ETL were deposited with heating to eliminate SOP. (b) External quantum efficiency (EQE) as a function of current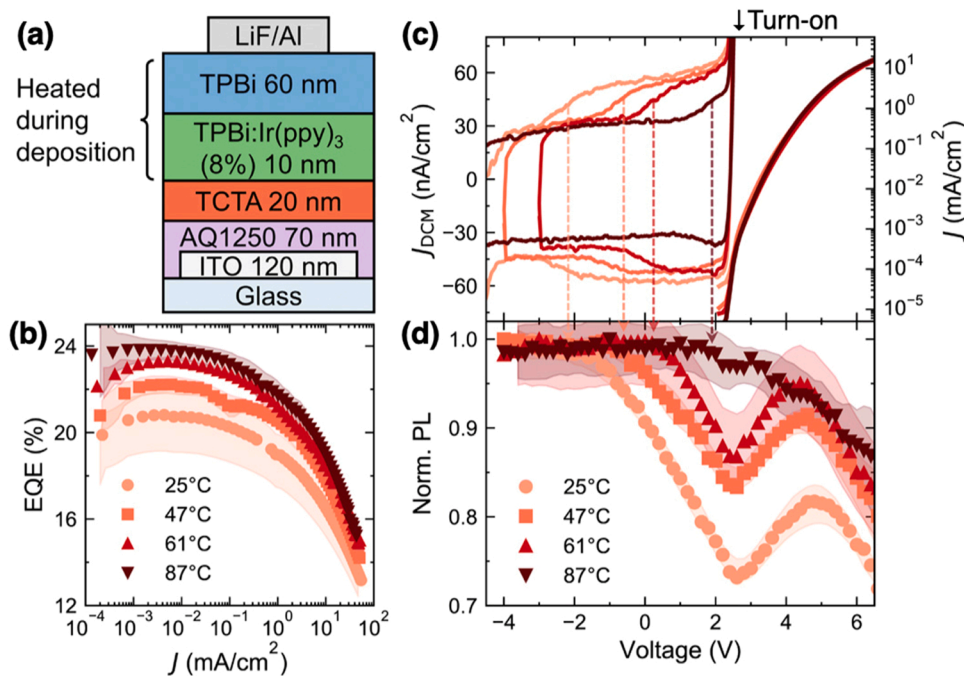 density. Higher EQEs are observed for the devices heated at higher temperatures. (c) DCM curves. The hole injection voltage shifts to the higher side for the heated devices, indicating that SOP is eliminated by heating. (d) Normalized PL intensity of Ir(ppy)$_3$ as a function of applied voltage. Significant PL drop is observed below turn-on, which is consistent with the hole injection behaviors in the DCM curves. Adapted from Ref. [45] under the terms of the CC-BY 4.0 license. Copyright 2020, The Authors, published by the American Association for the Advancement of Science.

At the Alq$_3$/NPB interface, the main quencher of the singlet exciton has been attributed to cationic NPB$^+$, because it has an absorption band around 500 nm [27]. On the other hand, Ir(ppy)$_3^+$ is likely the triplet quencher in the Ir(ppy)$_3$-based phosphorescent OLEDs [74]. SOP induces the accumulation of excess holes or electrons at the interface depending on the polarity and layer stacking, though the negative polarization charge is induced on the bottom side of the film in most cases [4]. To maximize the EQE of OLEDs, one should consider the density, polarity, and location of the interface charge with respect to the EML in the device stack.

The spatial distribution of the accumulated charge is also important because it directly influences the exciton-quenching probability. As a conventional technique, the Mott-Schottky analysis has often been used to determine the accumulated charge (or dopant) distribution in the bulk region [75–77]. A modified approach to evaluate the hole distribution at the interface region was proposed and applied to the NPB/Alq$_3$ interface [18]. The results suggest that the accumulated charge density decays exponentially from the interface, but it distributes to the middle of the NPB layer. As an alternative method, a combined analysis of DCM (or *C–V*) and PL quenching characteristics would be promising [46,60]. Bangsund et al. have estimated the hole distribution width at the CBP:Ir(ppy)$_3$/TPBi and TCTA/TPBi:Ir(ppy)$_3$ interfaces to be 3–4 nm by assuming an exponential decay of the accumulated charge density [46]. Actual devices involve rather complex situations, particularly at applied voltages above turn-on, and thus device simulations would be helpful for further understanding of the charge distribution including its dynamics under operational conditions [53,78].

3.2. Exciton dissociation

GSP typically decays via light absorption of the molecule [1,63]. This photoinduced decay nature was already reported in the first GSP paper [1]; however, the mechanism had been controversial for several years [22–25]. Two different mechanisms were mainly discussed; one is the light stimulated reorientation of molecules in the film, and the other is the photo-induced generation of the compensation charge while maintaining molecular orientation in the film. Although the properties of Alq$_3$ films had been mainly studied using Kelvin probe and optical second harmonic generation in the first several years, after identifying

SOP as the origin of the interface charge in OLEDs [2,3,15], the latter mechanism has been widely accepted. The fact indicates that SOP forms a sufficiently strong electric field to dissociate excitons generated in the film.

Yamanaka et al. reported that exciton dissociation even occurs spontaneously in a film which consists of a polar TADF molecule, that is, TPA-DCPP (13.05 D) doped with a CBP host (Fig. 9) [56]. When excitons are generated, part of them is dissociated due to the electric field formed by SOP in the doped film. The excited state is "stored" as separated electrons and holes in the film, and some of them result in "long-lived emission" with a lifetime of the order of milliseconds depending on the excitation pulse width. The separated charges remain at least for 1 h at the film interfaces as compensation charges of SOP.

Further studies of the spontaneous exciton dissociation were recently reported [52,57]. Ueda et al. investigated the dissociation of charge transfer excitons (CTE) in donor-acceptor blends, such as m-MTDATA: T2T and TAPC:T2T, where the m-MTDATA film exhibits larger SOP (15 mV/nm) than the TAPC film (4.3 mV/nm). Because the exciton binding energy of CTEs is weaker than Frenkel excitons, CTE dissociation is expected with relatively weak electric field. Spontaneous exciton dissociation was actually found in the m-MTDATA:T2T film due to the electric field of SOP, whereas that in the TAPC:T2T film is too small. As a result, the total PLQY of the m-MTDATA:T2T film (5%) appears much smaller than that of the TAPC:T2T film (75%).

The PL lifetime measured in polar films may include the contribution of long-lived emission via exciton dissociation due to SOP. Accordingly, the PLQY may be underestimated for analyzing device properties of OLEDs if spontaneous exciton dissociation occurs in a film, because the electric field of SOP is compensated at forward bias voltages in OLEDs under operation. On the other hand, this effect may act positively in applications like organic photovoltaics and organic long persistent luminescence systems [79].

3.3. Charge injection and accumulation

SOP induces polarization charges on both the top and bottom sides of a film, which have the same density but opposite polarity. If a film exhibiting SOP is used as an ETL, one should consider this polarization charge not only at the interface of the EML side, but also at the interface
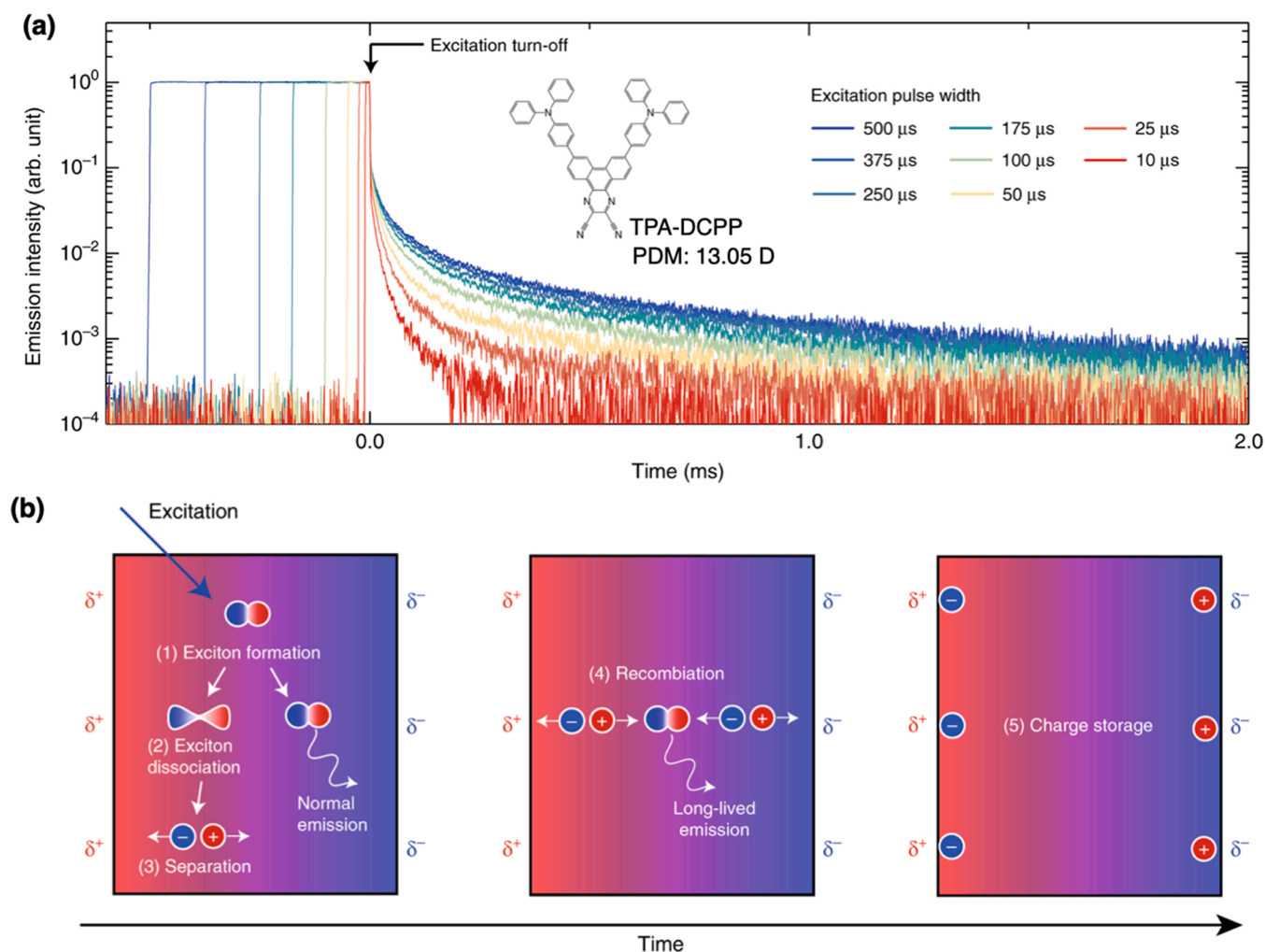
Fig. 9. (a) Dependence of time-resolved PL profile on excitation pulse width for a 50%-TPA-DCPP:CBP blend. Chemical structure of TPA-DCPP is also shown. A 470-nm light source was used as excitation light, and power density was fixed at 25 mW/cm². Longer lifetime of the long-tailed component is observed with increasing excitation pulse width, though it saturates for the pulse width longer than 375 μs. (b) Schematic of spontaneous exciton dissociation and recombination processes in solid films containing organic polar fluorophores. Reproduced from Ref. [55] under the terms of the CC-BY 4.0 license. Copyright 2019, The Authors.

of the cathode side. Noguchi et al. pointed out that the polarization charge at the ETL/cathode affects the electron injection efficiency, based on experimental results of Alq₃ and Al(7-prq)₃-based OLEDs, where Al (7-prq)₃ induces a negative polarization charge at the cathode side interface in contrast to Alq₃ [13]. The declining charge injection efficiency due to the negative polarization charge at the cathode interface, or vice versa, is also supported by simulation results based on drift-diffusion modeling [14], the observation of relaxed electron states [80], and a DCM study of electron-only MIS devices [55].

Hofmann et al. applied the concept of dipolar doping to enhance hole injection efficiency (Fig. 1) [51]. They comprehensively studied the electrical properties of the bulk and the interfaces of hole-only devices, where the mixed films consisting of NPB as a nonpolar host and Alq₃ as a polar dopant were employed as active layer. The dipolar doping of Alq₃ leads to SOP in the mixed film and the maximum hole injection efficiency appeared at a doping ratio of about 5% (0.4 mC/m²). It should be noted that SOP of most HTL materials is very small owing to their small PDM [4,54], thus dipolar doping would be useful to induce SOP in HTLs. Hofmann et al. also pointed out that this effect is valid when the initial energy offset is relatively high, as e.g. at the ITO/NPB interface [51]. Similarly, based on the results of a three-dimensional kinetic Monte Carlo simulation (3D KMC), Coehoorn et al. indicated that an improvement of electron injection efficiency due to SOP is only expected for a large energy barrier (> 0.6 eV), in the case of the TPBi/cathode

interface [53].

Coehoorn et al. reported a simulation study on the effects of PDM and its orientation on many aspects of OLED properties using 3D KMC, where TPBi is employed as a polar ETL material [53]. They calculated the electron and hole density profiles across the device in operation with varying SOP of TPBi. Interestingly, hole blocking at the EML/TPBi interface is imperfect when the negative polarization charge density is relatively high, leading to hole leakage and a loss of internal quantum efficiency (Fig. 1). The hole leakage could be attributed to the presence of the negative interface charge, since it may enhance "hole injection" into the TPBi layer. A photoelectron spectroscopy study suggests a similar positive charge transfer across organic/organic interfaces involving SOP layers (OXD-7 and TPBi), possibly due to the presence of negative interface charges [81].

Another important aspect accompanied by SOP is broadening of the density of states (DOS) of a polar film, though it originates from the microscopic potential fluctuations induced by disorder of PDMs (Fig. 1). The tail states of the broad DOS act as charge traps and reduce the charge carrier mobility of materials [53,82,83], while they assist in charge injection from the electrode [84]. On the other hand, the charge dispersion along the organic hetero interface consisting of polar films can be suppressed by the PDM-induced potential fluctuation [3,85]. Thus, besides macroscopic influences of SOP on charge injection and accumulation properties, one needs to take into account these dipolar

disorder effects that are inherent in amorphous films of polar materials.

4. Applications of SOP

4.1. SOP as a tool for evaluating material properties

To investigate the specific properties of device such as charge injection and transport, MIS structures and unipolar devices have been often used as a model system instead of the actual device structure [51, 55,62,77,86,87]. Charge blocking at organic/organic interfaces often relies on the energy offset of two materials. To block current leakage across the interface, insulating materials, such as SiO_2, PMMA, and so on, have been typically used, because of their wide energy gap (e.g., ~9 eV for SiO_2 [88], >5 eV for PMMA [89]). In unipolar devices, hole or electron blocking layers with a relatively deep highest occupied molecular orbital (HOMO) or shallow lowest unoccupied molecular orbital (LUMO) level have been widely used to restrict a specific charge current. However, the current insulation of such charge blocking layers would be insufficient. On the other hand, some excellent insulators can hardly be formed on organic layers without damaging them. A careful selection of the materials combinations as well as their layer stacks are often required.

Züfle et al. proposed a MIS-CELIV measurement to determine a material's charge carrier mobility, where an Alq_3 layer acts as an excellent charge blocking layer instead of usual wide-energy gap materials (Fig. 10) [58]. The charge blocking property of the Alq_3 layer relies on its SOP, where the interface charge guarantees charge accumulation of the opposite polarity without leakage current until it is compensated, regardless of the energy offset between the materials. They applied this concept to a typical Alq_3-based bilayer OLED and estimated the hole mobilities of NPB in this way. A similar concept was used to determine the hole transport activation energy and injection barrier by combining MIS-CELIV and capacitance-frequency-temperature measurements [59].

Another important aspect of SOP is molecular orientation, as it originates from the alignment of PDMs. Molecular orientation has already been widely accepted as key parameter to maximize the device performance of modern OLEDs [69,70]. Although molecular orientation has been often evaluated in terms of TDM alignment using optical

Fig. 10. (a) and (b) Schematic energy level diagram of bilayer devices, where (a) a conventional wide-energy gap material or (b) an SOP material is used as a charge blocking layer. (c) MIS-CELIV curves of an NPB/Alq_3 bilayer device. The hole extraction currents across the NPB layer are observed. Reproduced from Ref. [57] under the terms of the CC-BY 4.0 license. Copyright 2017, Author(s).

techniques such as variable angle spectroscopic ellipsometry (VASE) and angular dependent PL (ADPL) [69,70], measuring PDM orientation – if a given material has a non-vanishing electric dipole moment – can provide additional information. For instance, often films of some materials are isotropic in terms of TDM orientation, but anisotropic in terms of PDM orientation (e.g., Alq_3, see Fig. 5), and vice versa [10,50]. Furthermore, the combined analysis of TDM and PDM orientations would be useful to analyze SOP in mixed films consisting of multiple polar molecules [29, 40,61].

Morgenstern et al. have proposed a method of accurate determination of the orientation distribution of molecules based on the evaluations of both PDM and TDM alignment. They examined typical phosphorescent emitters, like $Ir(ppy)_3$ and $Ir(ppy)_2(acac)$, in a guest–host system (Fig. 11) [50]. The preferential alignment of $Ir(ppy)_2(acac)$ has a narrow orientation distribution of the molecular C_2 symmetry axis, with its maximum close to the normal direction, whereas $Ir(ppy)_3$ exhibits random orientation of its C_3 axis. Furthermore, the degree of aggregation in $Ir(ppy)_2(acac)$-based guest–host systems was also estimated, where aggregates with an anti-parallel PDM alignment are formed above 10% dye content and reduce SOP while keeping the TDM orientation unchanged.

Naqvi et al. have extended the combined study of PDM and TDM orientations to guest-host systems including TADF emitters and various polar host materials [29]. They examined the TDM orientation of TADF emitters by ADPL measurement as well as the PDM orientation of the host materials by Kelvin probe or impedance spectroscopy. From the correlations of TDM and PDM orientations, they pointed out three main factors for the formation of TADF emitter alignment that include their molecular shape, the T_g of the host material as well as the tendency of alignment of the host molecule, though the electrostatic PDM interaction between host and emitter is less important. The conclusions are consistent with those obtained from orientation analyses of phosphorescent emitters of Ir complexes [40].

4.2. SOP films as an electret material

Since SOP was first found in an Alq_3 film, as discussed in the previous sections, much research has been devoted to clarifying the mechanism of spontaneous orientation of polar molecules and the effect of polarization charges on OLED performance [4]. Alq_3 is, of course, a representative organic semiconducting material, but as has already been pointed out in the first GSP paper [1], Alq_3 films showing GSP can be regarded as an electret. An electret is a dielectric material with a quasi-permanent electrical charge or dielectric polarization and has been widely utilized as the foundation of air filters, microphones, sensors, and VEGs [66]. Among them, electret-based VEGs (E-VEGs), which can generate electrical power from ambient vibration, are of particular interest as an alternative to batteries for wireless sensor nodes [90–95]. There are several kinds of VEGs utilizing piezoelectric effect, electromagnetic inductions, etc., while the E-VEG is classified as an electrostatic energy generator. An advantage of E-VEG is that they can generate relatively high output voltage even at lower vibrational frequencies than around 100 Hz, which are widely available in the environment [92,95]. Further, E-VEGs are generally compatible with MEMS processes which enables the miniaturization of the device. The output power of E-VEGs is typically below 1 mW; however, the possibility of powering the wireless sensors by E-VEGs is growing mainly due to advances in low power processing and wireless communications.

E-VEGs typically have a capacitor structure in which vibrational and fixed electrodes sandwich electret and air-gap (Fig. 12(a)). In the E-VEGs, vibrations of the top electrode cause the air gap distance to change, thus changing the capacitance, causing charges to redistribute and generate a current which is proportional to the rate of change of the capacitance. In other words, the E-VEG acts like an AC voltage source wherein a DC voltage source composed of the electret is in series with a variable capacitor. The electrical charges on the electrodes are induced
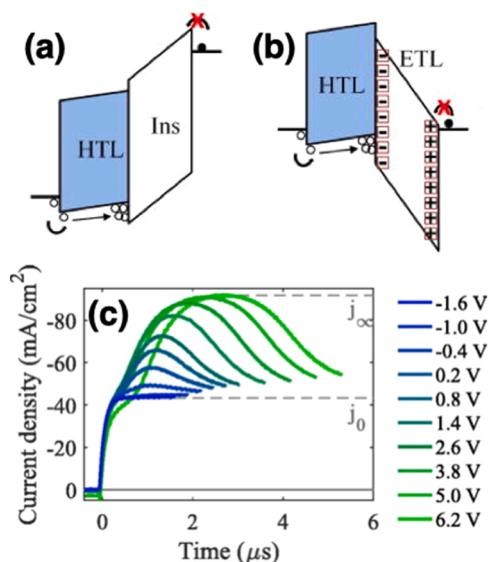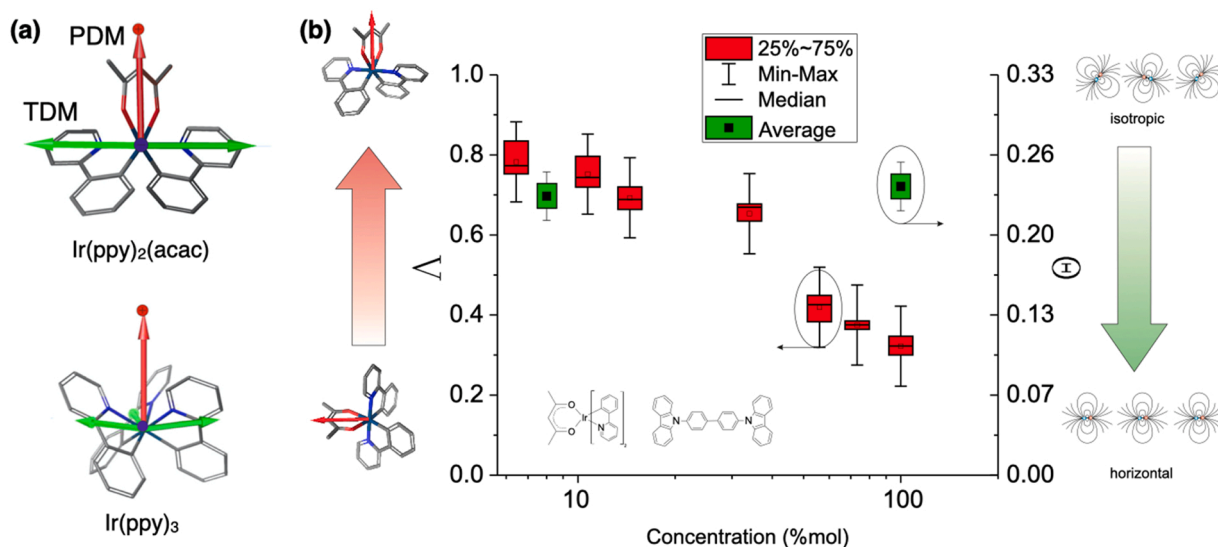
Fig. 11. (a) Three-dimensional molecular structure of Ir(ppy)$_2$(acac) (top) and Ir(ppy)$_3$ (bottom). The red and green arrows indicate PDM and TDM, respectively. (b) Experimentally determined orientation degrees of PDM (Λ) and TDM (Θ) values for Ir-(ppy)$_2$(acac) at various concentrations doped into CBP. Reproduced with permission from Ref. [49]. Copyright 2017, American Chemical Society.
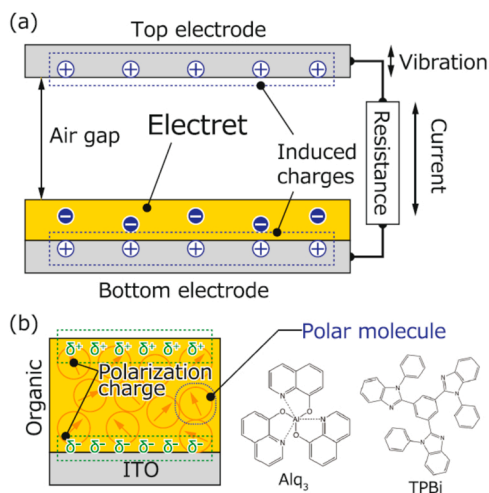

Fig. 12. Schematics of (a) E-VEG and (b) SAE film and chemical structure of Alq$_3$ and TPBi. Reproduced from Ref. [62] under the terms of the CC-BY 4.0 license. Copyright 2020, The Authors.

on the vibrational electrodes by the electric field formed by the electret, and thus the output power of the device is proportional to the square of the surface potential of the electret. Therefore the electret is a key material and indispensable for E-VEGs. But unfortunately, a charging process like corona discharge to dielectric materials is necessary for the fabrication of conventional electrets, leading to low productivity and high manufacturing costs of devices. Note that the charging process could be skipped by substituting conventional electrets with self-assembled electrets (SAEs), i.e. molecules exhibiting GSP such as Alq$_3$ and TPBi (Fig. 12(b)). Y. Tanaka et al. demonstrated that an SAE-based VEG generates current during vibration [63] and recently showed that the generated current is proportional to the surface potential of the SAE [96]. These results suggest that an increase in the film thickness can enhance the output power of the SAE-VEG. We will discuss adequate materials for SAE-VEG in the last two paragraphs of this section.

To realize the practical use of SAE-VEG as a power source for electronic devices, including wireless sensors, it is important to integrate SAEs with MEMS, which can downscale device size while increasing the output power per unit volume [97]. Conventional electrets can be integrated; however, there are limitations to MEMS designs and their fabrication processes, owing to the requirement of high voltages and/or high temperatures for electret preparation. Further, charging processes generally make monolithic integration of MEMS and electrical circuits challenging to fabricate using post-processing [98,99]. To overcome these, Yamane and co-workers recently demonstrated a MEMS VEG followed by post-processing the SAE [67]. In the proposed device, a SAE is deposited on the fixed electrode via through-holes provided to the movable (vibrational) one (Fig. 13(a) and (b)). As shown in Fig. 13(c), the output currents are generated during vibration and their intensities depend on the acceleration amplitudes as previously reported [100]. Further, the output current is attenuated after UV irradiation, indicating the contribution of GSP to the electrical power generation. The optimized load resistance is the MΩ range (Fig. 13(d)), that is comparable to the conventional electret-based MEMS VEGs [93,97]. With this integration technology, SAE-based MEMS VEG can be implemented with MEMS sensors, including wireless transceiver circuits, leading to single-chip autonomous wireless sensors.

Finally, let us discuss polar organic molecules suitable for E-VEGs. The electret's high surface potential is essential to realize E-VEGs with high output power because the power is proportional to the square of the potential. In conventional electrets composed of fluorinated polymers, the surface potential has reached approximately 1500 V after corona charging [65], while that of SAEs is only a few tens of volts [63], implying that a drastic improvement is needed. But the surface charge density of polymer electrets is approximately 2 mC/m^2, which is comparable to that of TPBi (1.7 mC/m^2): in other words, the difference in surface potential between the conventional electrets and SAEs is mainly due to the difference in film thickness. If the SAE thickness is increased to more than ten micrometers, which is equivalent to that of the polymer electret, a surface potential on the order of kV could be realized in SAEs. Thus, one can safely state that SAEs have the potential for practical use as an electret for E-VEGs. Nevertheless, it is essential to develop SAE films with a high charge density because the amount of the required material can be reduced, resulting in reductions in tact time and manufacturing costs. Combining dipolar doping, high dipole moment molecules, and molecular design to achieve preferred PDM orientation is key to achieving high-performing E-VEGs.

At the same time, if SAE-VEGs are supposed to perform in the field for distributed sensors, the long-term stability of SOP is an essential
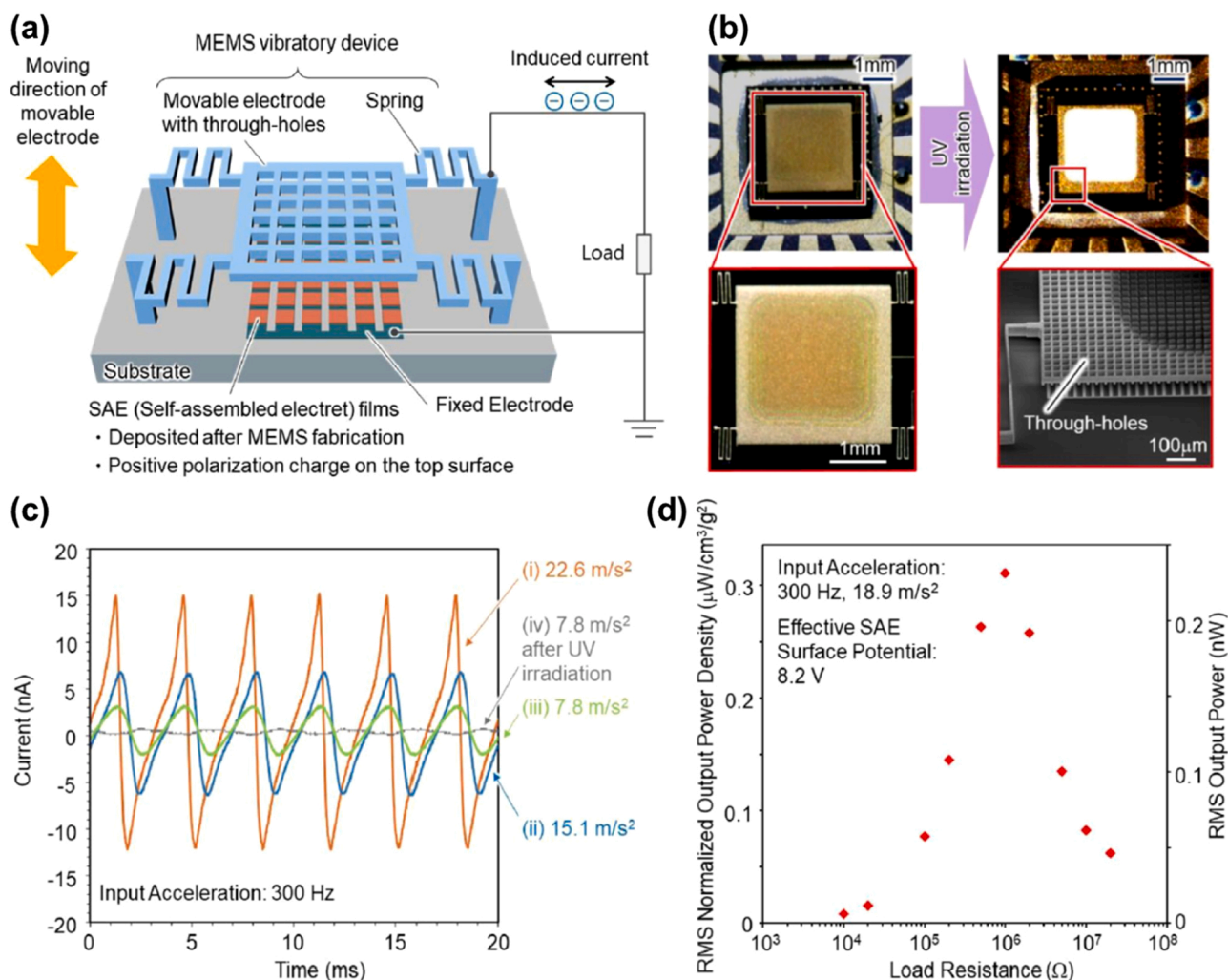
Fig. 13. (a) Schematic of the integration of the MEMS device and SAE. (b) Integration results of SAE and MEMS VEG using the MEMS post-process with or without UV light irradiation. (c) Output current waveforms under vibration with various acceleration. (d) Output power and its density as a function of load resistance. Reproduced with permission from Ref. [66]. Copyright 2021, Authors, AIP Publishing.

parameter. In fact, much effort has been devoted to evaluating and improving the stability of polymer-based electrets, and Kashiwagi et al. have demonstrated that the surface charge remained over 2500 h [65]. Although the retention time of the 10% loss in TPBi is approximately 140 h in the dark and air conditions [63], Sugi and co-workers showed that the SOP decay rate of Alq_3 was approximately 10 years for 10% loss in dark and vacuum conditions. Thus, developing new materials with long stability and/or encapsulation techniques for SAE-VEGs are vital for practical application. Similarly, thermal stability is also a key parameter and has been evaluated in polymer electrets by using a thermally stimulated discharge measurement [65,92]. In contrast, though studies about thermal stability for SOP are limited, Kajimoto et al. have reported that the surface potential of Alq_3 decreased at the substrate temperature higher than 100 ℃, resulting from randomization of dipole moments together with the injection of electrons from the metal substrate below the Alq_3 film [24]. Note that TPBi and Alq_3 show T_g of 129 ℃ and 177 ℃ [101], respectively, which are higher than the conventional polymer electrets (around 110 ℃ [65]). A relationship between T_g and thermal stability of SOP is still unclear. But we believe that molecular design developed for OLED materials to achieve high T_g are also applicable for high-performance SAEs.

5. Summary and outlook

Recent progress in the understanding of SOP and its applications to devices are reviewed. Over the years, the essential points of the formation mechanism of SOP have become clearer in terms of the surface equilibration mechanism of vapor-deposited glasses, where the key feature is an anisotropic layer formed on the film surface during deposition. From a microscopic viewpoint, the vdW interaction between molecules and the film surface is considered to be the main driving force, indicating that molecular shape, including conformers, and substituents at the outer part of a molecule play an important role. On the other hand, dipole-dipole interactions among PDMs typically reduce SOP.

SOP can be controlled by evaporation conditions, e.g., the substrate temperature and the deposition rate, and by the doping ratio of guest-host systems. Furthermore, light illumination during deposition is suggested to enhance SOP of films. In terms of molecular design, attaching substituents to a specific molecular framework would be promising to independently control the alignment of molecules and their PDM magnitude and polarity, and thus tuning their film SOP.

Recent progress in understanding the influence of SOP on device performance of OLEDs has gained considerable importance. In particular, significant exciton quenching due to the SOP-induced charge accumulation at EML interfaces has been demonstrated, suggesting there is room for further improvement of EQE by the active management

of SOP in the device stack. The charge accumulation characteristics at interfaces is also crucial in terms of efficiency roll-off and device lifetime.

SOP has attracted increasing attention in recent years. Our understanding of SOP and its influences on OLED characteristics have progressed significantly. We should consider to manage SOP for optimizing device performance. A fine-tuning method of the interface charge density as well as the appropriate choice of polar and non-polar materials would be key issues. From the viewpoint of applications, the demonstration of a vibrational energy generator composed of materials showing SOP represents an important step. Further applications are expected for utilizing this class of materials.

Finally, we comment on some next challenges. Although many OLED materials exhibit SOP, most of them are ETLs or emitters. Polar HTLs would extend possible device stacks in terms of controlling charge accumulation in them. Similarly, only few materials are known to exhibit negative SOP, which induces a negative polarization charge on the film surface. To establish molecular design rules to control SOP while keeping key materials functionality would open a new concept of OLED device architectures. On the other hand, dipolar disorder and SOP have been studied independently in most cases. Understanding the effect of SOP on DOS broadening may be another challenge. It would also be important to reveal how large SOPs can be achieved, since in many cases PDM alignment is significantly quenched in terms of their averaged orientation degree, e.g., $\langle \cos\theta_p \rangle < 0.1$; however, the largest GSP slope ever reported is 163 mV/nm for a film of BCPO, corresponding to $\langle \cos\theta_p \rangle$ of 0.33 [29]. Exploring materials with extremely large SOP as well as their robustness under environmental conditions are obviously important for the applications of SAEs. Such materials could potentially be used as ferroelectric or piezoelectric materials, too, and enable new emerging organic semiconductor devices.

Declaration of Competing Interest

The authors declare that they have no known competing financial interests or personal relationships that could have appeared to influence the work reported in this paper.

Acknowledgments

References

[1] E. Ito, Y. Washizu, N. Hayashi, H. Ishii, N. Matsuie, K. Tsuboi, Y. Ouchi, Y. Harima, K. Yamashita, K. Seki, Spontaneous buildup of giant surface potential by vacuum deposition of Alq3 and its removal by visible light irradiation, J. Appl. Phys. 92 (2002) 7306, https://doi.org/10.1063/1.1518759.

[2] Y. Noguchi, N. Sato, Y. Tanaka, Y. Nakayama, H. Ishii, Threshold voltage shift and formation of charge traps induced by light irradiation during the fabrication of organic light-emitting diodes, Appl. Phys. Lett. 92 (2008), 203306, https://doi.org/10.1063/1.2936084.

[3] Y. Noguchi, Y. Miyazaki, Y. Tanaka, N. Sato, Y. Nakayama, T.D. Schmidt, W. Brütting, H. Ishii, Charge accumulation at organic semiconductor interfaces due to a permanent dipole moment and its orientational order in bilayer devices, J. Appl. Phys. 111 (2012), 114508, https://doi.org/10.1063/1.4724349.

[4] Y. Noguchi, W. Brütting, H. Ishii, Spontaneous orientation polarization in organic light-emitting diodes, Jpn. J. Appl. Phys. 58 (2019) SF0801, https://doi.org/10.7567/1347-4065/ab0de8.

[5] S. Berleb, W. Brütting, G. Paasch, Interfacial charges and electric field distribution in organic hetero-layer light-emitting devices, Org. Electron. 1 (2000) 41–47, https://doi.org/10.1016/S1566-1199(00)00007-0.

[6] W. Brütting, S. Berleb, A.G. Mückl, Device physics of organic light-emitting diodes based on molecular materials, Org. Electron. 2 (2001) 1–36, https://doi.org/10.1016/S1566-1199(01)00009-X.

[7] W. Brütting, H. Riel, T. Beierlein, W. Riess, Influence of trapped and interfacial charges in organic multilayer light-emitting devices, J. Appl. Phys. 89 (2001) 1704–1712, https://doi.org/10.1063/1.1332088.

[8] N. Hayashi, K. Imai, T. Suzuki, K. Kanai, Y. Ouchi, K. Seki, Substrate dependence of giant surface potential of Alq3 and examination of surface potential of related materials, in: Proceedings of the International Symposium on Super-Functionality Organic Devices, IPAP Conference, 2004, pp. 69–72. ⟨http://www.ipap.jp/proc/cs6/pdf/cs6_069.pdf⟩.

[9] M. Kröger, S. Hamwi, J. Meyer, T. Dobbertin, T. Riedl, W. Kowalsky, H. H. Johannes, Temperature-independent field-induced charge separation at doped organic/organic interfaces: experimental modeling of electrical properties, Phys. Rev. B Condens. Matter Mater. Phys. 75 (2007), 235321, https://doi.org/10.1103/PhysRevB.75.235321.

[10] K. Osada, K. Goushi, H. Kaji, C. Adachi, H. Ishii, Y. Noguchi, Observation of spontaneous orientation polarization in evaporated films of organic light-emitting diode materials, Org. Electron. 58 (2018) 313–317, https://doi.org/10.1016/J.ORGEL.2018.04.026.

[11] Y. Noguchi, N. Sato, Y. Miyazaki, Y. Nakayama, H. Ishii, Higher resistance to hole injection and electric field distribution in organic light-emitting diodes with copper phthalocyanine interlayer, Jpn. J. Appl. Phys. 49 (2010) 01AA01, https://doi.org/10.1143/JJAP.49.01AA01.

[12] T.D. Schmidt, L. Jäger, Y. Noguchi, H. Ishii, W. Brütting, Analyzing degradation effects of organic light-emitting diodes via transient optical and electrical measurements, J. Appl. Phys. 117 (2015), 215502, https://doi.org/10.1063/1.4921829.

[13] Y. Noguchi, H. Lim, T. Isoshima, E. Ito, M. Hara, W. Won Chin, J. Wook Han, H. Kinjo, Y. Ozawa, Y. Nakayama, H. Ishii, Influence of the direction of spontaneous orientation polarization on the charge injection properties of organic light-emitting diodes, Appl. Phys. Lett. 102 (2013), 203306, https://doi.org/10.1063/1.4807797.

[14] S. Altazin, S. Züfle, E. Knapp, C. Kirsch, T.D. Schmidt, L. Jäger, Y. Noguchi, W. Brütting, B. Ruhstaller, Simulation of OLEDs with a polar electron transport layer, Org. Electron. Phys. Mater. Appl. 39 (2016) 244–249, https://doi.org/10.1016/j.orgel.2016.10.014.

[15] Y. Noguchi, N. Sato, Y. Miyazaki, H. Ishii, Light- and ion-gauge-induced space charges in tris-(8-hydroxyquinolate) aluminum-based organic light-emitting diodes, Appl. Phys. Lett. 96 (2010), 143305, https://doi.org/10.1063/1.3374405.

[16] D.Y. Kondakov, J.R. Sandifer, C.W. Tang, R.H. Young, Nonradiative recombination centers and electrical aging of organic light-emitting diodes: Direct connection between accumulation of trapped charge and luminance loss, J. Appl. Phys. 93 (2003) 1108, https://doi.org/10.1063/1.1531231.

[17] V.V. Jarikov, D.Y. Kondakov, Studies of the degradation mechanism of organic light-emitting diodes based on tris(8-quinolinolate)aluminum Alq and 2-tert-butyl-9,10-di(2-naphthyl)anthracene TBADN, J. Appl. Phys. 105 (2009), 034905, https://doi.org/10.1063/1.3072622.

[18] Y. Noguchi, T. Tamura, H. Kim, H. Ishii, Device properties of Alq3-based organic light-emitting diodes studied by displacement current measurement, J. Photonics Energy 2 (2012), 021214, https://doi.org/10.1117/1.JPE.2.021214.

[19] S. Nowy, W. Ren, A. Elschner, W. Lövenich, W. Brütting, Impedance spectroscopy as a probe for the degradation of organic light-emitting diodes, J. Appl. Phys. 107 (2010), 054501, https://doi.org/10.1063/1.3294642.

[20] Y. Noguchi, H. Kim, R. Ishino, K. Goushi, C. Adachi, Y. Nakayama, H. Ishii, Charge carrier dynamics and degradation phenomena in organic light-emitting diodes doped by a thermally activated delayed fluorescence emitter, Org. Electron. 17 (2015) 184–191, https://doi.org/10.1016/j.orgel.2014.12.009.

[21] A. Hofmann, M. Schmid, W. Brütting, The many facets of molecular orientation in organic optoelectronics, Adv. Opt. Mater. 9 (2021) 2101004, https://doi.org/10.1002/adom.202101004.

[22] K. Sugi, H. Ishii, Y. Kimura, M. Niwano, E. Ito, Y. Washizu, N. Hayashi, Y. Ouchi, K. Seki, Characterization of light-erasable giant surface potential built up in evaporated Alq3 thin films, Thin Solid Films 464–465 (2004) 412–415, https://doi.org/10.1016/j.tsf.2004.06.035.

[23] K. Yoshizaki, T. Manaka, M. Iwamoto, Large surface potential of Alq3 film and its decay, J. Appl. Phys. 97 (2005), 023703, https://doi.org/10.1063/1.1835543.

[24] N. Kajimoto, T. Manaka, M. Iwamoto, Decay process of a large surface potential of Alq3 films by heating, J. Appl. Phys. 100 (2006), 053707, https://doi.org/10.1063/1.2338137.

[25] T. Manaka, K. Yoshizaki, M. Iwamoto, Investigation of the surface potential formed in Alq3 films on metal surface by Kelvin probe and nonlinear optical measurement, Curr. Appl. Phys. 6 (2006) 877–881, https://doi.org/10.1016/j.cap.2005.06.004.

[26] T. Miyamae, N. Takada, T. Yoshioka, S. Miyaguchi, H. Ohata, T. Tsutsui, Rearrangement of the molecular orientation of Alq3 in organic light-emitting diodes under constant current aging investigated using sum frequency generation spectroscopy, Chem. Phys. Lett. 616–617 (2014) 86–90, https://doi.org/10.1016/j.cplett.2014.10.027.

[27] A.P. Marchetti, T.L. Haskins, R.H. Young, L.J. Rothberg, Permanent polarization and charge distribution in organic light-emitting diodes (OLEDs): insights from near-infrared charge-modulation spectroscopy of an operating OLED, J. Appl. Phys. 115 (2014), 114506, https://doi.org/10.1063/1.4867779.

[28] J. ichi Takahashi, H. Naito, Visualization of the carrier transport dynamics in layered organic light emitting diodes by modulus spectroscopy, Org. Electron. 61 (2018) 10–17, https://doi.org/10.1016/j.orgel.2018.06.056.

[29] B.A. Naqvi, M. Schmid, E. Crovini, P. Sahay, T. Naujoks, F. Rodella, Z. Zhang, P. Strohriegl, S. Bräse, E. Zysman-Colman, W. Brütting, What controls the orientation of TADF emitters? Front. Chem. 8 (2020) 750, https://doi.org/10.3389/fchem.2020.00750.

[30] K. Bagchi, N.E. Jackson, A. Gujral, C. Huang, M.F. Toney, L. Yu, J.J. De Pablo, M. D. Ediger, Origin of anisotropic molecular packing in vapor-deposited Alq3 glasses, J. Phys. Chem. Lett. 10 (2019) 164–170, https://doi.org/10.1021/acs.jpclett.8b03582.

[31] M.D. Ediger, J. De Pablo, L. Yu, Anisotropic vapor-deposited glasses: hybrid organic solids, Acc. Chem. Res. 52 (2019) 407–414, https://doi.org/10.1021/acs.accounts.8b00513.

[32] K. Bagchi, M.D. Ediger, Controlling structure and properties of vapor-deposited glasses of organic semiconductors: recent advances and challenges, J. Phys. Chem. Lett. 11 (2020) 6935–6945, https://doi.org/10.1021/acs.jpclett.0c01682.

[33] P. Friederich, V. Rodin, F. Von Wrochem, W. Wenzel, Built-in potentials induced by molecular order in amorphous organic thin films, ACS Appl. Mater. Interfaces 10 (2018) 1881–1887, https://doi.org/10.1021/acsami.7b11762.

[34] Y. Noguchi, K. Osada, K. Ninomiya, H.D.C.N. Gunawardana, K.R. Koswattage, H. Ishii, Influence of intermolecular interactions on the formation of spontaneous orientation polarization in organic semiconducting films, J. Soc. Inf. Disp. 29 (2021) 29–37, https://doi.org/10.1002/jsid.956.

[35] L. Jäger, T.D. Schmidt, W. Brütting, Manipulation and control of the interfacial polarization in organic light-emitting diodes by dipolar doping, AIP Adv. 6 (2016), 095220, https://doi.org/10.1063/1.4963796.

[36] T. Isoshima, Y. Okabayashi, E. Ito, M. Hara, W.W. Chin, J.W. Han, Negative giant surface potential of vacuum-evaporated tris(7-propyl-8-hydroxyquinolinolato) aluminium(III) [Al(7-Prq)3] film, Org. Electron. Phys. Mater. Appl. 14 (2013) 1988–1991, https://doi.org/10.1016/j.orgel.2013.04.032.

[37] H.D.C.N. Gunawardana, K. Osada, K.R. Koswattage, Y. Noguchi, Enhancement of the molecular orientation of TPBi in coevaporated films of UGH-2 host molecules, Surf. Interface Anal. 53 (2021) 460–465, https://doi.org/10.1002/sia.6933.

[38] Y. Sukegawa, K. Sato, W. Fujiwara, H. Katagiri, D. Yokoyama, Effect of the conformer distribution on the properties of amorphous organic semiconductor films for organic light-emitting diodes, Phys. Chem. Chem. Phys. 23 (2021) 14242–14251, https://doi.org/10.1039/d1cp00892g.

[39] Y. Sukegawa, Y. Sakai, D. Yokoyama, Model-free analysis of molecular orientation in amorphous organic semiconductor films for understanding its formation dynamics: methods and systematic investigation, Org. Electron. 100 (2022), 106377, https://doi.org/10.1016/j.orgel.2021.106377.

[40] M. Schmid, K. Harms, C. Degitz, T. Morgenstern, A. Hofmann, P. Friederich, H. H. Johannes, W. Wenzel, W. Kowalsky, W. Brütting, Optical and electrical measurements reveal the orientation mechanism of homoleptic iridium-carbene complexes, ACS Appl. Mater. Interfaces 12 (2020) 51709–51718, https://doi.org/10.1021/acsami.0c14613.

[41] M.J. Jurow, C. Mayr, T.D. Schmidt, T. Lampe, P.I. Djurovich, W. Brütting, M. E. Thompson, Understanding and predicting the orientation of heteroleptic phosphors in organic light-emitting materials, Nat. Mater. 15 (2016) 85–91, https://doi.org/10.1038/nmat4428.

[42] C.K. Moon, K.H. Kim, J.J. Kim, Unraveling the orientation of phosphors doped in organic semiconducting layers, Nat. Commun. 8 (2017) 791, https://doi.org/10.1038/s41467-017-00804-0.

[43] M.C. Jung, J. Facendola, J. Kim, D.S. Muthiah Ravinson, P.I. Djurovich, S. R. Forrest, M.E. Thompson, Molecular alignment of homoleptic iridium phosphors in organic light-emitting diodes, Adv. Mater. 33 (2021) 2102882, https://doi.org/10.1002/adma.202102882.

[44] M. Tanaka, M. Auffray, H. Nakanotani, C. Adachi, Spontaneous formation of metastable orientation with well-organized permanent dipole moment in organic glassy films, Nat. Mater. (2022), https://doi.org/10.1038/s41563-022-01265-7.

[45] W.-C. Wang, K. Nakano, D. Hashizume, C.-S. Hsu, K. Tajima, Tuning molecular conformations to enhance spontaneous orientation polarization in organic thin films, ACS Appl. Mater. Interfaces (2022), https://doi.org/10.1021/acsami.2c03496.

[46] J.S. Bangsund, J.R. Van Sambeek, N.M. Concannon, R.J. Holmes, Sub-turn-on exciton quenching due to molecular orientation and polarization in organic light-emitting devices, Sci. Adv. 6 (2020), https://doi.org/10.1126/sciadv.abb2659 eabb2659.

[47] Y. Esaki, M. Tanaka, T. Matsushima, C. Adachi, Active control of spontaneous orientation polarization of tris(8-hydroxyquinolinato)aluminum (Alq3) films and its effect on performance of organic light-emitting diodes, Adv. Electron. Mater. 7 (2021), 2100486, https://doi.org/10.1002/aelm.202100486.

[48] Y. Tanaka, N. Matsuura, H. Ishii, Enhancement of output power in self-assembled electret-based vibrational energy generator: control of molecular orientation by changing deposition rate, in: Proceedings of the PowerMEMS 2019, 2020, SubID: 41031605688. ⟨https://doi.org/10.1109/powermems49317.2019.41031605688⟩.

[49] Y. Tanaka, Y. Tazo, H. Ishii, Enhanced orientation of 1,3,5-tris (1-phenyl-1H-benzimidazole-2-yl)benzene by light irradiation during its deposition evaluated by displacement current measurement, IEICE Trans. Electron. E104-C (2021) 176–179, https://doi.org/10.1587/transele.2020OMS0009.

[50] T. Morgenstern, M. Schmid, A. Hofmann, M. Bierling, L. Jäger, W. Brütting, Correlating optical and electrical dipole moments to pinpoint phosphorescent dye alignment in organic light-emitting diodes, 31541–311, ACS Appl. Mater. Interfaces 10 (2018), https://doi.org/10.1021/acsami.8b08963.

[51] A.J.L. Hofmann, S. Züfle, K. Shimizu, M. Schmid, V. Wessels, L. Jäger, S. Altazin, K. Ikegami, M.R. Khan, D. Neher, H. Ishii, B. Ruhstaller, W. Brütting, Dipolar doping of organic semiconductors to enhance carrier injection, Phys. Rev. Appl. 12 (2019), 064052, https://doi.org/10.1103/PhysRevApplied.12.064052.

[52] Y. Ueda, H. Nakanotani, T. Hosokai, Y. Tanaka, H. Hamada, H. Ishii, S. Santo, C. Adachi, Role of spontaneous orientational polarization in organic donor–acceptor blends for exciton binding, Adv. Opt. Mater. 8 (2020), 2000896, https://doi.org/10.1002/adom.202000896.

[53] R. Coehoorn, X. Lin, C.H.L. Weijtens, S. Gottardi, H. van Eersel, Three-dimensional modeling of organic light-emitting diodes containing molecules with large electric dipole moments, Phys. Rev. Appl. 16 (2021), 034048, https://doi.org/10.1103/physrevapplied.16.034048.

[54] S. Sato, M. Takada, D. Kawate, M. Takata, T. Kobayashi, H. Naito, Interfacial charges and electroluminescence in bilayer organic light-emitting diodes with different hole transport materials, Jpn. J. Appl. Phys. 58 (2019), https://doi.org/10.7567/1347-4065/ab0de7. SFFA02.

[55] Y. Tanaka, T. Makino, H. Ishii, Influence of polarity of polarization charge induced by spontaneous orientation of polar molecules on electron injection, IEICE Trans. Electron. E102-C (2019) 172–175, https://doi.org/10.1587/transele.2018OMS0014.

[56] T. Yamanaka, H. Nakanotani, C. Adachi, Slow recombination of spontaneously dissociated organic fluorophore excitons, Nat. Commun. 10 (2019) 5748, https://doi.org/10.1038/s41467-019-13736-8.

[57] T. Yamanaka, H. Nakanotani, C. Adachi, Significant role of spin-triplet state for exciton dissociation in organic solids, Sci. Adv. 8 (2022), https://doi.org/10.1126/sciadv.abj9188 eabj9188.

[58] S. Züfle, S. Altazin, A. Hofmann, L. Jäger, M.T. Neukom, T.D. Schmidt, W. Brütting, B. Ruhstaller, The use of charge extraction by linearly increasing voltage in polar organic light-emitting diodes, J. Appl. Phys. 121 (2017), 175501, https://doi.org/10.1063/1.4982903.

[59] S. Züfle, S. Altazin, A. Hofmann, L. Jäger, M.T. Neukom, W. Brütting, B. Ruhstaller, Determination of charge transport activation energy and injection barrier in organic semiconductor devices, J. Appl. Phys. 122 (2017), 115502, https://doi.org/10.1063/1.4992041.

[60] T. Ferschke, A. Hofmann, W. Brütting, J. Pflaum, Application of fluorescent molecules as non-invasive sensors for opto-electronic characterization on nanometer length scales, ACS Appl. Electron. Mater. 2 (2020) 186–194, https://doi.org/10.1021/acsaelm.9b00687.

[61] M. Tanaka, H. Noda, H. Nakanotani, C. Adachi, Molecular orientation of disk-shaped small molecules exhibiting thermally activated delayed fluorescence in host – guest films, Appl. Phys. Lett. 116 (2020), 023302, https://doi.org/10.1063/1.5140210.

[62] A. Armin, G. Juska, M. Ullah, M. Velusamy, P.L. Burn, P. Meredith, A. Pivrikas, Balanced carrier mobilities: not a necessary condition for high-efficiency thin organic solar cells as determined by MIS-CELIV, Adv. Energy Mater. 4 (2014), 1300954, https://doi.org/10.1002/aenm.201300954.

[63] Y. Tanaka, N. Matsuura, H. Ishii, Self-assembled electret for vibration-based power generator, Sci. Rep. 10 (2020) 6648, https://doi.org/10.1038/s41598-020-63484-9.

[64] N. Matsuura, H. Ishii, Y. Tanaka, Demonstration of an electret generator using self-assembled electret for energy harvesting without any charging process, J. Phys. Conf. Ser. 1407 (2019), 012116, https://doi.org/10.1088/1742-6596/1407/1/012116.

[65] K. Kashiwagi, K. Okano, T. Miyajima, Y. Sera, N. Tanabe, Y. Morizawa, Y. Suzuki, Nano-cluster-enhanced high-performance perfluoro-polymer electrets for energy harvesting, J. Micromech. Microeng. 21 (2011) 125016, https://doi.org/10.1088/0960-1317/21/12/125016.

[66] G.M. Sessler. Erectlets, third ed., Laplacian Press, 1998.

[67] D. Yamane, H. Kayaguchi, H. Kawashima, H. Ishii, Y. Tanaka, MEMS post-processed self-assembled electret for vibratory energy harvesters, Appl. Phys. Lett. 119 (2021), 254102, https://doi.org/10.1063/5.0072596.

[68] C.W. Tang, S.A. Vanslyke, Organic electroluminescent diodes, Appl. Phys. Lett. 51 (1987) 913–915, https://doi.org/10.1063/1.98799.

[69] D. Yokoyama, Molecular orientation in small-molecule organic light-emitting diodes, J. Mater. Chem. 21 (2011) 19187, https://doi.org/10.1039/c1jm13417e.

[70] T.D. Schmidt, T. Lampe, M.R. Daniel Sylvinson, P.I. Djurovich, M.E. Thompson, W. Brütting, Emitter orientation as a key parameter in organic light-emitting diodes, Phys. Rev. Appl. 8 (2017), 037001, https://doi.org/10.1103/PhysRevApplied.8.037001.

[71] M. Shibata, Y. Sakai, D. Yokoyama, Advantages and disadvantages of vacuum-deposited and spin-coated amorphous organic semiconductor films for organic light-emitting diodes, J. Mater. Chem. C 3 (2015) 11178–11191, https://doi.org/10.1039/C5TC01911G.

[72] M. Ohara, T. Watanabe, Y. Tanaka, H. Ishii, Examination of spontaneous orientation polarization in wet-processed tris(8-hydroxyquinolinato)aluminum film measured by rotary Kelvin probe method, Phys. Status Solidi Appl. Mater. Sci. 218 (2021), 2000790, https://doi.org/10.1002/pssa.202000790.

[73] C. Murawski, K. Leo, M.C. Gather, Efficiency roll-off in organic light-emitting diodes, Adv. Mater. 25 (2013) 6801–6827, https://doi.org/10.1002/adma.201301603.

[74] S. Oyama, H. Sakai, H. Murata, Rate constant of exciton quenching of Ir(ppy)3 with hole measured by time-resolved luminescence spectroscopy, Jpn. J. Appl. Phys. 55 (2016) 03DD13, https://doi.org/10.7567/JJAP.55.03DD13.

[75] E.J. Meijer, A.V.G. Mangnus, C.M. Hart, D.M. De Leeuw, T.M. Klapwijk, Frequency behavior and the Mott-Schottky analysis in poly(3-hexyl thiophene)

metal-insulator-semiconductor diodes, Appl. Phys. Lett. 78 (2001) 3902–3904, https://doi.org/10.1063/1.1378803.

[76] I. Torres, D.M. Taylor, Interface states in polymer metal-insulator-semiconductor devices, J. Appl. Phys. 98 (2005), https://doi.org/10.1063/1.2081109.

[77] S. Demura, T. Endo, T. Ishii, D. Yokoyama, Y. Noguchi, Molecular orientation anisotropy and hole transport properties of diluted semiconducting films of poly (p-phenylenevinylene) derivative, Org. Electron. 96 (2021), 106246, https://doi.org/10.1016/j.orgel.2021.106246.

[78] S. Jenatsch, S. Züfle, B. Blülle, B. Ruhstaller, Combining steady-state with frequency and time domain data to quantitatively analyze charge transport in organic light-emitting diodes, J. Appl. Phys. 127 (2020), 031102, https://doi.org/10.1063/1.5132599.

[79] R. Kabe, C. Adachi, Organic long persistent luminescence, Nature 550 (2017) 384–387, https://doi.org/10.1038/nature24010.

[80] H. Kinjo, H. Lim, T. Sato, Y. Noguchi, Y. Nakayama, H. Ishii, Significant relaxation of residual negative carrier in polar Alq3 film directly detected by high-sensitivity photoemission, Appl. Phys. Express 9 (2016), 021601, https://doi.org/10.7567/APEX.9.021601.

[81] Y. Nakayama, S. Machida, Y. Miyazaki, T. Nishi, Y. Noguchi, H. Ishii, Electronic structures at organic heterojunctions of N,N′-bis(1- naphthyl)-N,N′-diphenyl-1,1′-biphenyl-4,4′-diamin (NPB)-based organic light emitting diodes, Org. Electron. Phys. Mater. Appl. 13 (2012) 2850–2855, https://doi.org/10.1016/j.orgel.2012.08.033.

[82] P.M. Borsenberger, E.H. Magin, M. Der Van Auweraer, F.C. De Schryver, The role of disorder on charge transport in molecularly doped polymers and related materials, Phys. Status Solidi 140 (1993) 9–47, https://doi.org/10.1002/pssa.2211400102.

[83] A. Dieckmann, H. Bässler, P.M. Borsenberger, An assessment of the role of dipoles on the density-of-states function of disordered molecular solids, J. Chem. Phys. 99 (1993) 8136–8141, https://doi.org/10.1063/1.465640.

[84] M. Baldo, S. Forrest, Interface-limited injection in amorphous organic semiconductors, Phys. Rev. B 64 (2001), 085201, https://doi.org/10.1103/PhysRevB.64.085201.

[85] J. Veres, S.D. Ogier, S.W. Leeming, D.C. Cupertino, S.M. Khaffaf, Low-k insulators as the choice of dielectrics in organic field-effect transistors, Adv. Funct. Mater. 13 (2003) 199–204, https://doi.org/10.1002/adfm.200390030.

[86] D. Yokoyama, T. Sasaki, Y. Suzuki, T. Abe, K. Tsuruoka, T. Miyajima, T. Kakiuchi, C. Morita, M. Aoki, Y. Ouchi, W. Aita, Y. Kuwana, Y. Noguchi, Active refractive index control using a stably evaporable perfluororesin for high-outcoupling-efficiency organic light-emitting diodes, J. Mater. Chem. C 9 (2021) 11115–11125, https://doi.org/10.1039/d1tc02478g.

[87] Y. Noguchi, Y. Tanaka, Y. Miyazaki, N. Sato, Y. Nakayama, H. Ishii, Displacement current measurement for exploring charge carrier dynamics in organic semiconductor devices, in: W. Brütting, C. Adachi (Eds.), Physics of Organic Semiconductors, second ed., Wiley-VCH, 2012, pp. 119–154.

[88] J. Robertson, Band offsets of wide-band-gap oxides and implications for future electronic devices, J. Vac. Sci. Technol. B Microelectron. Nanom. Struct. 18 (2000) 1785, https://doi.org/10.1116/1.591472.

[89] C. Wu, F. Li, T. Guo, Efficient tristable resistive memory based on single layer graphene/insulating polymer multi-stacking layer, Appl. Phys. Lett. 104 (2014), 183105, https://doi.org/10.1063/1.4875596.

[90] H. Akinaga, Recent advances and future prospects in energy harvesting technologies, Jpn. J. Appl. Phys. 59 (2020), 110201, https://doi.org/10.35848/1347-4065/abbfa0.

[91] M. Shirvanimoghaddam, K. Shirvanimoghaddam, M.M. Abolhasani, M. Farhangi, V. Zahiri Barsari, H. Liu, M. Dohler, M. Naebe, Towards a green and self-powered internet of things using piezoelectric energy harvesting, IEEE Access 7 (2019) 94533–94556, https://doi.org/10.1109/ACCESS.2019.2928523.

[92] Y. Suzuki, Recent progress in MEMS electret generator for energy harvesting, IEEJ Trans. Electr. Electron. Eng. 6 (2011) 101–111, https://doi.org/10.1002/tee.20631.

[93] Y. Suzuki, D. Miki, M. Edamoto, M. Honzumi, A MEMS electret generator with electrostatic levitation for vibration-driven energy-harvesting applications, J. Micromech. Microeng. 20 (2010), 104002, https://doi.org/10.1088/0960-1317/20/10/104002.

[94] S.P. Beeby, M.J. Tudor, N.M. White, Energy harvesting vibration sources for microsystems applications, Meas. Sci. Technol. 17 (2006) R175–R195, https://doi.org/10.1088/0957-0233/17/12/R01.

[95] S. Roundy, P.K. Wright, J. Rabaey, A study of low level vibrations as a power source for wireless sensor nodes, Comput. Commun. 26 (2003) 1131–1144, https://doi.org/10.1016/S0140-3664(02)00248-7.

[96] Y. Tanaka, N. Matsuura, H. Ishii, Current generation mechanism in self-assembled electret-based vibrational energy generators, Sens. Mater. 34 (2022) 1859–1867, https://doi.org/10.18494/SAM3860.

[97] H. Honma, H. Mitsuya, G. Hashiguchi, H. Fujita, H. Toshiyoshi, Improvement of energy conversion effectiveness and maximum output power of electrostatic induction-type MEMS energy harvesters by using symmetric comb-electrode structures, J. Micromech. Microeng. 28 (2018), 064005, https://doi.org/10.1088/1361-6439/aab514.

[98] C.Y. Chen, M.H. Li, S.S. Li, CMOS-MEMS resonators and oscillators: a review, Sens. Mater. 30 (2018) 733–756, https://doi.org/10.18494/SAM.2018.1857.

[99] Y.C. Liu, M.H. Tsai, T.L. Tang, W. Fang, Post-CMOS selective electroplating technique for the improvement of CMOS-MEMS accelerometers, J. Micromech. Microeng. 21 (2011), 105005, https://doi.org/10.1088/0960-1317/21/10/105005.

[100] K. Tao, S.W. Lye, J. Miao, L. Tang, H. Xiao, Out-of-plane electret-based MEMS energy harvester with the combined nonlinear effect from electrostatic force and a mechanical elastic stopper, J. Micromech. Microeng. 25 (2015), 104014, https://doi.org/10.1088/0960-1317/25/10/104014.

[101] J.Y. Shen, C.Y. Lee, T.H. Huang, J.T. Lin, Y.T. Tao, C.H. Chien, C. Tsai, High Tg blue emitting materials for electroluminescent devices, J. Mater. Chem. 15 (2005) 2455–2463, https://doi.org/10.1039/b501819f.